CHAOS DETECTION TOOLS: THE LP-VICODE AND ITS APPLICATIONS (PRELIMINAR VERSION OF THE PAPER)

Luciano Darriba
Grupo de Caos en Sistemas Hamiltonianos - FCAGLP
Universidad Nacional de La Plata
Argentina
ldarriba@fcaglp.unlp.edu.ar

Nicolás Maffione
Grupo de Caos en Sistemas Hamiltonianos - FCAGLP
Universidad Nacional de La Plata
Argentina
nmaffione@fcaglp.unlp.edu.ar

Pablo Cincotta
Grupo de Caos en Sistemas Hamiltonianos - FCAGLP
Universidad Nacional de La Plata
Argentina
pmc@fcaglp.unlp.edu.ar

Claudia Giordano
Grupo de Caos en Sistemas Hamiltonianos - FCAGLP
Universidad Nacional de La Plata
Argentina
giordano@fcaglp.unlp.edu.ar

Abstract

A very important topic in galactic dynamics is the detection of instabilities of a given system and the possible appearance of chaos. Such a chaotic bahaviour can be detected and studied by means of variational chaos indicators (CIs). The CIs are based on the study of the evolution of initial deviation vectors, which makes these techniques specially sensitive to indicate the presence of chaos.

Herein, we present an alpha version of a program coded in Fortran, the LP-VIcode. Although the code is in a developing stage, it can compute several CIs, and here we apply it together with the Frequency Modified Fourier Transform (FMFT) ([Sidlichovský and Nesvorný, 1996]) to study the stationary space ([Schwarzschild, 1993]) of an average realistic Hamiltonian model ([Muzzio, Carpintero and Wachlin, 2005]).

Using the LP-VIcode, in [Maffione, Darriba, Cincotta and Giordano, 2011b] and [Darriba, Maffione, Cincotta and Giordano, 2012] the authors suggest an efficient package of CIs to study a general Hamiltonian. Here the research is extended to show that the complementary use of the LP-VIcode and the spectral analysis methods is highly recommended to study a realistic Hamiltonian model.

Key words

Chaos detection; dynamical systems; numerical techniques

1 Introduction

The detection of chaotic behaviour in any dynamical system, such as galaxies or planetary systems, may be carried out by means of several techniques. The most commonly used are those based on spectral analysis and on the study of the evolution of the deviation vectors, the so-called variational chaos indicators (CIs hereafter). Among the CIs we can find several examples: the Lyapunov Indicators (LIs) (see [Benettin, Galgani and Stralcyn, 1976]; [Benettin, Galgani, Giorgilli and Strelcyn, 1980]; [Froeschlé, 1984]; [Tancredi, Sánchez and Roig, 2001] and [Skokos, 2010]), the Relative Lyapunov Indicator (RLI) (see [Sándor, Érdi and Efthymiopoulos, 2000]; [Széll, Érdi, Sándor and Steves, 2004]; [Sándor, Érdi, Széll and Funk, 2004] and [Sándor, Süli, Érdi, Pilat-Lohinger and Dvorak, 2007]), and the Smaller Alignment Index (SALI) ([Skokos, 2001]; [Széll, Érdi, Sándor and Steves, 2004]; [Bountis and Skokos, 2006]; [Carpintero, 2008]; [Antonopoulos, Vasileios and Bountis, 2010]). All of them have their own advantages and disadvantages, making them particularly suitable for different situations.

It could be very interesting and fruitful to have the possibility of easily computing *any* CI. This is the main goal of the first part of this work where we present an alpha version of the LP-VIcode (the acronym for La Plata-Variational Indicators code). The aim of the code, as its name suggests, is to easily compute several CIs and, for instance, in [Maffione, Darriba, Cincotta and Giordano, 2011b] (hereafter M11) and [Darriba, Maffione, Cincotta and Giordano, 2012] (hereafter D12), the authors use it to make a comparative evaluation among them in order to analize

the main advantages and drawbacks of each indicator. On the other hand, in the second part of this work we present the results of the application of the CIs implemented within the code, together with a spectral analysis method, to show that the complementary use of both types of chaos detection tools is strongly advisable.

As the CIs are based on the concept of local exponential divergence, they are specially sensitive to indicate the presence of chaos. The introduction of the Lyapunov Characteristic Exponents (LCEs) (see e.g. [Skokos, 2010] for a current thorough discussion) as well as its numerical implementation ([Benettin, Galgani, Giorgilli and Strelcyn, 1980]; [Skokos, 2010]) was a major contribution to the advance of chaos detection. The integration time is bounded, so we are able to reach just truncated approximations of the theoretical LCEs, i.e. the already mentioned LIs. A drawback of the computation of the LIs is their very slow speed of convergence. Nevertheless, since the introduction of the first definition of the LI, a large number of CIs have improved the LIs' slow speed of convergence holding many useful characteristics of it. The following CIs are already implemented in the `LP-VIcode` with the LI: the Mean Exponential Growth factor of Nearby Orbits (MEGNO) ([Cincotta and Simó]; [Cincotta, Giordano and Simó, 2003]; [Giordano and Cincotta, 2004]; [Goździewski, Konacki and Maciejewski, 2005]; [Gayon and Bois, 2008]; [Lemaître, Delsate and Valk, 2009]; [Hinse, Christou, Alvarellosn and Gózdziewski, 2010]; [Maffione, Giordano and Cincotta, 2011a]; [Comére, Lemaître and Delsate, 2011]) and a quantity derived from it: the MEGNO's Slope Estimation of the largest LCE (SEILCE), the SALI and its generalized version, the Generalized Alignment Index (GALI) ([Skokos, Bountis and Antonopoulos, 2007]; [Skokos, Bountis and Antonopoulos, 2007]; [Manos and Athanassoula, 2011]), the Fast Lyapunov Indicator (FLI) ([Froeschlé, Gonczi and Lega, 1997a]; [**?**]; [Froeschlé and Lega, 1998]; [Froeschlé and Lega, 2000]; [Lega and Froeschlé, 2001]; [Guzzo, Lega and Froeschlé, 2002]; [Froeschlé and Lega, 2006]; [Paleari, Froeschlé and Lega, 2008]; [Todorović, Lega and Froeschlé, 2008]; [Lega, Guzzo and Froeschlé, 2010]), its first order variant, the Orthogonal Fast Lyapunov Indicator (OFLI) ([Fouchard, Lega, Foreschlé and Froeschlé, 2002]) and its second order variant, the OFLI_2^{TT} ([Barrio, 2005]; [Barrio, Blesa and Serrano, 2009]; [Barrio, Blesa and Serrano, 2010]); the Spectral Distance (*D*) ([Voglis, Contopoulos and Efthymiopoulos, 1999]) and the Dynamical Spectras of Stretching Numbers (SSNs) ([Voglis and Contopoulos, 1994]; [Contopoulos and Voglis, 1996]; [Contopoulos and Voglis, 1997]; [Contopoulos, Voglis, Efthymiopoulos Froeschlé, Gonczi, Lega, Dvorak and Lohinger, 1997]; [**?**]). Finally, we have also implemented the RLI and the Average Power Law Exponent (APLE) ([Lukes-Gerakopoulos, Voglis and Efthymiopoulos, 2008]). The RLI is not based on the evolution of the solution of the first variational equations as the rest of the variational indicators implemented, but on the evolution of two different but very close orbits. The APLE is based on the concept of Tsallis Entropy.

The other widespread techniques devoted to chaos detection are the analysis of some particular quantities (e.g. the frequency) of a single orbit. The main contributions in the area of chaos detection is due to [Binney and Spergel, 1982] and [Laskar, 1990] (see also [Laskar, Froeschlé and Celetti, 1992]; [Papaphilippou and Laskar, 1996]; [**?**]). The Frequency Modified Fourier Transform (FMFT) outlined by [Sidlichovský and Nesvorný, 1996] is another example of such kind of technique. The FMFT is the spectral analysis method selected for this investigation.

As previously mentioned, in M11 the authors compare the CIs implemented in an early version of the `LP-VIcode` on symplectic mappings. In D12, the authors use a later version of the `LP-VIcode` (where the CIs library was increased). Therefore, they do not only extend the work on mappings to a simple Hamiltonian flow: the [Hénon and Heiles, 1964] potential, but also they increase the number of CIs considered in the comparison. Both works deal with a comparative evaluation of the following CIs: the LI, the MEGNO, the SALI and the GALIs (GALI_k with $k = 2, 3, 4$), the FLI and the OFLI, the *D* and the SSNs and the RLI on symplectic mappings and a Hamiltonian flow. Finally, they suggest an efficient set of CIs (or CI's function which they call CIsF) composed by the pair FLI/OFLI, the MEGNO and the GALI_{2N} to study a general N–degree of freedom (d.o.f.) Hamiltonian system. In a work in progress, we use the latest version of the `LP-VIcode`, and do some experiments in a somehow realistic model of a triaxial stellar Hamiltonian system ([Muzzio, Carpintero and Wachlin, 2005]; [Cincotta, Giordano and Muzzio, 2008]). The `LP-VIcode` latest version library of CIs includes all the CIs mentioned in the earlier versions of the code, plus the SEILCE, the OFLI_2^{TT} and the APLE. We extend the previous comparative studies of the CIs and find that the CIsF to study a general Hamiltonian system can be improved considering the pair FLI/OFLI, the pair MEGNO/SEILCE and the OFLI_2^{TT} or the GALI_{2N}. The pair FLI/OFLI and the pair MEGNO/SEILCE are recommended to study big samples of orbits by means of just computing their final values. The OFLI_2^{TT} or the GALI_{2N} are suggested to study small regions of very complex dynamics or regions dominated by strong chaos ([Skokos, Bountis and Antonopoulos, 2007]; [Skokos, Bountis and Antonopoulos, 2008]; D12), respectively. However, here we are going to test the CIs against a spectral analysis method on two regions of the stationary and the $x_0 - z_0$ start spaces ([Schwarzschild, 1993]) of the self–consistent triaxial stellar Hamiltonian model previously mentioned. In

order to do so, we use one of the recommended CIs to study big samples of orbits, i.e. the MEGNO/SEILCE, and the LI (both techniques already implemented in the `LP-VIcode`) and the FMFT as the selected spectral analysis method.

This paper is organized as follows: in Section 2 we present the code and explain its main features. In Section 3 we apply the `LP-VIcode` to study a realistic model. In order to investigate the advantages and drawbacks of the selected CIs included in this version of the `LP-VIcode` and the FMFT, we apply both types of chaos detection techniques to study the same space and compare the results in Section 4

2 The `LP-VIcode`

The `LP-VIcode` (in its alpha version) computes several CIs. It was coded in `FORTRAN 77`, although it is intended to be recoded in `FORTRAN 90` on a later version.

Although the current version of the code is in a developing stage, it has already implemented twelve indicators, already named in Section 1 The record is: the LI, the RLI, the SALI, the GALI$_k$, the MEGNO, the SEILCE, the FLI, the OFLI, the OFLI$_2^{TT}$, the *D*, the SSNs and the APLE.

2.1 The CIs implemented in the `LP-VIcode`

2.1.1 The Lyapunov Indicator (LI). Consider a continuous dynamical system defined on a differentiable manifold $\mathcal{S}$, where $\vec{\Phi}^t(\vec{x}) = \vec{x}(t)$ characterizes the state of the system at time t, $\vec{x}(0) = \vec{x}_0$ being the state of the system at time $t = 0$. Therefore, the state of the system after two consecutive time steps t and t' will be given by the composition law: $\vec{\Phi}^{t+t'} = \vec{\Phi}^t \circ \vec{\Phi}^{t'}$.

The tangent space of $\vec{x}$ maps onto the tangent space of $\vec{\Phi}^t(\vec{x})$ according to the operator $d_{\vec{x}}\vec{\Phi}^t$ and following the rule $\vec{w}(t) = d_{\vec{x}}\vec{\Phi}^t(\vec{w}(0))$ where $\vec{w}(0)$ is an initial deviation vector. The action of such operator at consecutive time intervals satisfies the equation:

$$d_{\vec{x}}\vec{\Phi}^{t+t'} = d_{\vec{\Phi}^{t'}(\vec{x})}\vec{\Phi}^t \circ d_{\vec{x}}\vec{\Phi}^{t'}.$$

If we suppose that our manifold $\mathcal{S}$ has some norm denoted by $\|\cdot\|$, we can define the quantity:

$$\lambda_t(\vec{x}) = \frac{\|d_{\vec{x}}\vec{\Phi}^t\vec{w}\|}{\|\vec{w}\|}$$

called "growth factor" in the direction of $\vec{w}$.

Consider an N-dimensional Hamiltonian $H(\vec{p},\vec{q})$, with $\vec{p},\vec{q} \in \mathbb{R}^N$, which we consider it autonomous just for the sake of simplicity. Let us remember that

$$\vec{x} = (\vec{p},\vec{q}) \in \mathbb{R}^{2N}, \vec{f}(\vec{x}) = (-\partial H/\partial\vec{q}, \partial H/\partial\vec{p}) \in \mathbb{R}^{2N},$$

and then, the equations of motion are

$$\dot{\vec{x}} = \vec{f}(\vec{x}). \tag{1}$$

Let $\gamma(\vec{x_0};t)$ be an arc of the orbit in the flux given by equation (1) over a compact energy surface: $M_h \subset \mathbb{R}^{2N}$, $M_h = \{\vec{x} : H(\vec{p},\vec{q}) = h\}$ with h a constant, then

$$\gamma(\vec{x_0};t) = \vec{x}(t';\vec{x_0}) : \vec{x_0} \in M_h, 0 \leq t' < t.$$

We define the LCE χ:

$$\chi[\gamma(\vec{x_0};t)] = \lim_{t\to\infty} \frac{1}{t} \ln \lambda_t[\gamma(\vec{x}_0;t)], \tag{2}$$

and for its numerical implementation in the `LP-VIcode` we take the finite time limit of Eq. (2);

$$LI = \lim_{t\to T} \frac{1}{t} \ln \lambda_t[\gamma(\vec{x}_0;t)],$$

with T a finite time.

2.1.2 The Relative Lyapunov Indicator (RLI). If we graph the fluctuations of the LI, they are not significative. Thus, in order to amplify those fluctuations [Sándor, Érdi, Széll and Funk, 2004] define the quantity:

$$\Delta LI(\vec{x_0};t) = \|LI(\vec{x_0} + \vec{\Delta x};t) - LI(\vec{x_0};t)\|,$$

where $\vec{x_0}$ and $\vec{x_0} + \vec{\Delta x_0}$ are two very close initial conditions at time t, separated by a quantity $|\vec{\Delta x}|$, which is a free parameter. Then, the RLI is defined through the expression:

$$RLI(t) =< \Delta LI(\vec{x_0}) >_t = \frac{1}{t}\sum_{i=1}^{t/\delta_t} \Delta LI(\vec{x_0}, i\times\delta_t), \tag{3}$$

with i the number of steps of stepsize δ_t. We use the expression (3) in the `LP-VIcode` in order to compute the RLI.

2.1.3 The Dynamical Spectra of the Stretching Numbers (SSNs) and the Spectral Distance (D). The local stretching number s_i is defined as:

$$s_i = \frac{1}{\delta_t} \ln \frac{|d_{\vec{x}} \vec{\Phi}^{t+i\times\delta_t}(\vec{\omega}(0))|}{|d_{\vec{x}} \vec{\Phi}^{t+(i-1)\times\delta_t}(\vec{\omega}(0))|}, \tag{4}$$

where $d_{\vec{x}} \vec{\Phi}^{t+i\times\delta_t}(\vec{\omega}(0)) = \vec{\omega}(t + i \times \delta_t)$ is the deviation vector at time $t + i \times \delta_t$.

Then, the SSNs are given by the density probability of the values s given by the s_i, i.e.

$$S(s)ds = \frac{dN(s)}{N}, \tag{5}$$

where N is the total number of s_i and $dN(s)$ is the number of s_i in the interval $(s, s + ds)$. Thus, the computing of the SSNs in the `LP-VIcode` is just the construction of these histograms.

Then, the *D* is computed as the difference of two histograms of a given orbit. That is

$$D^2 = \sum_s [S_1(s) - S_2(s)]^2 \times \Delta s, \tag{6}$$

where $S_j(s)$ is the normalized number of s_i associated to the initial deviation vector $\vec{\omega}_j(0)$, which has values in the interval $s, s + \Delta s$.

The implementation of both the SSNs and the D in the `LP-VIcode` is based on the work of [Voglis, Contopoulos and Efthymiopoulos, 1999] and summarized by Eqs. (4), (5) and (6).

2.1.4 The Mean Exponential Growth Factor of Nearby Orbits (MEGNO) and the MEGNO's Slope Estimation of the largest Lyapunov Characteristic Exponent (SEILCE). The concept of local mean exponential rate of divergence of nearby orbits becomes evident when we rewrite the value of the LCE (Eq. 2) in an integral fashion:

$$\chi[\gamma(\vec{x}_0; t)] = \lim_{t\to\infty} \frac{1}{t} \int_0^t \frac{\|\dot{d_\gamma} \vec{\Phi}^{t'} \vec{w}\|}{\|d_\gamma \vec{\Phi}^{t'} \vec{w}\|} dt'.$$

Then, [Cincotta and Simó] defined the value Y as

$$Y[\gamma(\vec{x}_0; t)] = \frac{2}{t} \int_0^t \frac{\|\dot{d_\gamma} \vec{\Phi}^{t'} \vec{w}\|}{\|d_\gamma \vec{\Phi}^{t'} \vec{w}\|} t' dt'.$$

Finally, they introduced the MEGNO define as the average of Y, i.e.:

$$\overline{Y}[\gamma_q(\vec{x_0})] \equiv \frac{1}{t} \int_0^t Y[\gamma_q(\vec{x_0}; t')] dt'. \tag{7}$$

Having the value of the MEGNO (Eq. (7)), [Cincotta, Giordano and Simó, 2003] suggest a linear behaviour to enclose the MEGNO's performances for regular and chaotic orbits,

$$\overline{Y}[\gamma(\vec{x_0}; t)] \approx a_\gamma t + b_\gamma, \tag{8}$$

where $a_\gamma = \chi_\gamma/2$ and $b_\gamma \approx 0$ for irregular, chaotic motion, while $a_\gamma = 0$ and $b_\gamma \approx 2$ for quasiperiodic motion.

The SEILCE takes the last 80% of the time series samplings and makes a linear least square fit, in order to estimate the value of χ through the MEGNO behaviour given by Eq. (8).

The `LP-VIcode` computes the MEGNO following the Eq. (7), and makes the least square fit to recover the Eq. (8) and compute the SEILCE.

2.1.5 The Smaller Alignment Index (SALI) and the Generalized Alignment Index (GALI). In [Skokos, 2001], the authors introduce the SALI in the following way: first they define the parallel and antiparallel index

$$d_- = \|\vec{\omega}_1 - \vec{\omega}_2\|, \qquad d_+ = \|\vec{\omega}_1 + \vec{\omega}_2\|, \tag{9}$$

respectively. Then, they define the SALI at a time t as the lowest of these two indexes:

$$SALI(t) = \min(d_+, d_-). \tag{10}$$

In [Skokos, Bountis and Antonopoulos, 2007], the SALI is generalized, introducing the GALI as

$$GALI_k(t) = \|\hat{w}_1(t) \wedge \hat{w}_2(t) \wedge \cdots \wedge \hat{w}_k(t)\|,$$

where $\hat{w}_i(t) = \frac{\vec{w}_i(t)}{\|\vec{w}_i(t)\|}, i = 1, 2, \ldots, k$ is the normalized deviation vector.

As the computing of the GALI is very expensive in computational terms, [**?**] introduced a variation for the numerical computation of the GALI_k by making use of the singular value decomposition (SVD routine) of matrices and found that

$$\log(GALI_k) = \sum_{i=1}^{k} \log(z_i), \tag{11}$$

where the z_i are singular values of a given matrix Z.

The `LP-VIcode` computes the SALI following Eq. (10) and the GALI using the SVD routine of Numerical Recipes[1] to calculate the indicator through Eq. (11).

2.1.6 The Fast Lyapunov Indicator (FLI) and the Orthogonal Fast Lyapunov Indicator (OFLI). The FLI is a quantity closely related to the LI, which can distinguish between chaotic and regular motion ([Froeschlé, Gonczi and Lega, 1997a]; [Froeschlé, Lega and Gonczi, 1997b]) and even between resonant and non-resonant motion ([Froeschlé and Lega, 2000]; [Lega and Froeschlé, 2001]; [Guzzo, Lega and Froeschlé, 2002]) using (just) the first part of the numerical computing of the largest LCE.

For an N-dimensional system, in the `LP-VIcode` we follow the time evolution of the $2N$ deviation vectors and take the (euclidean) norm of each one. Then we record every K time steps, the largest of the norms, i.e. at time t the FLI is computed as

$$FLI(t) = \sup_t \left[\|\vec{w}_1(t)\|, \|\vec{w}_2(t)\|, \ldots, \|\vec{w}_{2N}(t)\| \right]. \tag{12}$$

As to the OFLI (see [Fouchard, Lega, Foreschlé and Froeschlé, 2002]), it is similar to the FLI, but in this case we take the orthogonal component to the flow of each deviation vector of the basis, time to time. Then it is defined as

$$OFLI(t) = \sup_t \left[w_1(t)^\perp, w_2(t)^\perp, \ldots, w_{2N}(t)^\perp \right]. \tag{13}$$

Notice that, although in the `LP-VIcode` we initially use the original definition of the FLI given in [Froeschlé, Gonczi and Lega, 1997a], to define the OFLI, we later included the definition of the FLI given in [Froeschlé and Lega, 2000], where the authors use only one deviation vector. As they claim, the results do not vary, but the CPU-time is obviously reduced. Finally, the OFLI can be also computed using just one deviation vector, following the definition given in [Fouchard, Lega, Foreschlé and Froeschlé, 2002].

2.1.7 The OFLI$^2_{TT}$. In [Barrio, 2005] the author defines the OFLI$^2_{TT}$, a second order variational indicator, as follows:

$$OFLI^2_{TT}(t) = \sup_{0<t<t_f} \hat{w}(t)^\perp,$$

$\hat{w}(t)^\perp$ being the orthogonal component of the flow of $\hat{\vec{w}}(t)$, where $\hat{\vec{w}}(t)$

$$\hat{\vec{w}}(t) = \vec{w}(t) + \frac{1}{2}\vec{w}^{(2)}(t)$$

$\vec{w}(t)$ and $\vec{w}^{(2)}(t)$ being the solutions of the first and second order variational equations at time t, respectively.

Finally, in the `LP-VIcode` we take the superior $\hat{w}(t)^\perp$ in the interval $(0, t_f]$ for a given total time t_f. For further details, we refer to [Barrio, 2005]; [Barrio, Blesa and Serrano, 2009]; [Barrio, Blesa and Serrano, 2010].

2.1.8 The Average Power Law Exponent (APLE). This method is based on the concept of Tsallis Entropy, thoroughly explained in [Lukes-Gerakopoulos, Voglis and Efthymiopoulos, 2008]. Thus, here we limit ourselves to show the formula we use to compute the indicator in the `LP-VIcode`.

For an N–dimensional Hamiltonian, these authors consider a partitioning of the $2N$–dimensional phase space $\mathcal{S}$ into a large number of volume elements of size δ^{2N} for some small δ and let $\vec{x}(0)$ be the initial condition of an orbit located in a particular volume element. Thus, they introduce the APLE as follows:

$$APLE = \frac{\ln\left(\frac{|\vec{w}(t)|^2}{|\vec{w}(t_1)|^2}\right)}{2\ln\left(\frac{t}{t_1}\right)},$$

where $|\vec{w}(t)|^2 = \sum_{k=1}^{m} \|\vec{w}_k(t)\|^2$, and $\vec{w}_k(t)$ is one of the m deviation vectors of an orthogonal basis $\{\vec{w}_k(t)\}$ of the tangent space to $\mathcal{S}$ at the initial point $\vec{x}(0)$. Every $\vec{w}_k(t)$ has a length greater or equal to δ, and t_1 is a transient initial time of the evolution of the orbits.

2.2 The arrangement of CIs in units

As the dynamics of a given Hamiltonian should be analysed using different techniques, providing a variety of CIs in the `LP-VIcode` proves advantageous.

Nearly all the CIs mentioned in Section 2.1 are completely independent from each other and can be computed separately. The only exceptions are the SEILCE, which it strictly depends on the MEGNO values to do the least square fit, and the RLI (which is the difference between the LI of two close orbits). Nevertheless, the main drawback of computing them separately is the huge amount of CPU time required. An alternative to reduce such a time-consuming process is to arrange the CIs according to (the similarity in) their computation. That is, although nearly all indicators can be computed independently, some of them share some basic routines. For instance, both the FLI and the OFLI use the evolution of the same $2N$ deviation vectors, N being the number of degrees

[1] See [Skokos, Bountis and Antonopoulos, 2008] for further details.

of freedom of the system[2]. Therefore, we decided to group the CIs in units the indicators sharing part of their computing processes.
This grouping is ordered as follows: the RLI is implemented in the same unit as the LI because it is the difference between the LI for two close initial conditions. Furthermore, the SALI is implemented in the same unit as the LI and the RLI, since it uses the evolution of the length of 2 deviation vectors. This is done in order to share the routine that computes the evolution of the deviation vectors which uses a renormalization process. Because the SEILCE (as mentioned before) uses the MEGNO to estimate the LI of the orbit, both CIs, the MEGNO and the SEILCE belong to the same unit. The FLI, the OFLI and the APLE can be computed using the same deviation vectors ($2N$ or just one, depending on the definition). Moreover, all of them use a routine that computes the evolution of the deviation vectors without the renormalization process previously used with the LI, RLI or SALI. The SSNs are basically built on the computation of histograms, and the *D* uses the difference of the SSNs for two different deviation vectors of a given orbit. Then, both of them are included in the same unit. The $GALI_k$ is computed in a different unit, due to the fact that it is the only CI using the SVD routine (see Section 2.1). The OFLI_2^{TT} is in a separate unit because it is the only CI that needs the computation of the second order variational equations, which requires the evaluation of third order derivatives.

Finally, the CIs implemented so far are arranged in the `LP-VIcode` as follows:

Unit 1: LI, RLI and SALI
Unit 2: MEGNO and SEILCE
Unit 3: FLI, OFLI and APLE
Unit 4: SSN and *D*
Unit 5: GALI_k
Unit 6: OFLI_2^{TT}

2.3 The input files

The `LP-VIcode` needs two input files in order to work. One of these files is a parameter file, in which all the information about the calibration of the indicators as well as the format of the output files is introduced. The other one is an input data file, which indicates which orbits we would have to compute.

2.3.1 The parameter file. Nearly all parameters can be set from this parameter file and only a few are still remain in the main program (mainly related with the specific problem). The main structure of this file consists of two parts. The first one arranges the input and output filenames and the second one arranges the parameters themselves. These parameters are the following:

Physical parameter: the energy of the system (in case the user does not specify all the initial condition coordinates of the phase space).
RLI parameter: the initial separation of both orbits (see Section 2.1).
Output parameter: a binary value to set which output is preferred in the computation, i.e. "0" only the final value of the CI (i.e. the value of the indicator at the end of the computing process) and "1" the time evolution of the CI.
Trajectory parameter: a binary value to print the phase space coordinates of the orbit ("1"), or skip the time-consuming writing process ("0").
CIs' selection parameter: a set of integer values to specify which units or CIs are to be computed.
Formatting parameters.

The CIs' selection parameter is one of the key parameters of the code, because it allows us to compute several CIs (with the efficient grouping mentioned before) to reduce the CPU time (see Section 2.2), or to compute them separately. The parameter is a horizontal array of 6 integers (one for each unit) which indicates the program if a given unit should be computed (value set equal to "1") or not (value set equal to "0"). In the case of the second unit (the MEGNO and the SEILCE), "1" is adopted so as to compute the MEGNO alone and "2" to compute the MEGNO and the SEILCE together.

2.3.2 The data file. The data file has a very simple format. In the first commented line, the order in which the program will read the data values is specified, i.e. the cartesian coordinates, the conjugate momentums and, the total integration time.

2.4 The Integrator

There are a lot of Ordinary Differential Equations (ODEs) integrators which can be implemented in the `LP-VIcode`, and the independency from the integrator routine is part of a future implementation. On the other hand, all the indicators already implemented in the code must integrate not only the equations of motion but also the first (and second) variational equations. Therefore, we need to count on an efficient integrator for these tasks. For instance, according to D12, a suitable integrator routine is the Prince & Dormand implementation of a Runge-Kutta method of order $7-8$ called DOPRI8 (for more information see [Prince and Dormand, 1981]. Thus, the DOPRI8 routine is the ODEs integrator selected for the current version of the `LP-VIcode`.

[2] According to the orginal definition given in [Froeschlé, Gonczi and Lega, 1997a], they can use the same deviation vector, according to the actual definition given in [Froeschlé and Lega, 2000], see Section 2.1 for further details.

3 Applications

In order to compare both types of chaos detection techniques (i.e. the variational and the frequency-based ones), we apply the MEGNO/SEILCE and the LI as representatives of the variational indicators implemented in the `LP-VIcode` and the FMFT, which is the selected spectral analysis method. Thus, in this section we are going to use the `LP-VIcode` and a spectral analysis method as complementary tools to study two regions of the stationary and the $x_0 - z_0$ start spaces ([Schwarzschild, 1993]) of the model introduced in [Muzzio, Carpintero and Wachlin, 2005] which will be briefly described in the next section.

3.1 The potential

The self–consistent triaxial Hamiltonian model of an elliptical galaxy is obtained after the virialization of an N–body self–consistent system composed of 10^5 particles ([Muzzio, Carpintero and Wachlin, 2005]). The model reproduces many dynamical characteristics of real elliptical galaxies, such as mass distribution, flattening, triaxiality and rotation ([Muzzio, 2006]). Therefore, it seems to provide a useful realistic scenario to apply the `LP-VIcode` and the FMFT as well.

The equation that reproduces the potential is

$$V(x,y,z) = -f_0(x,y,z) - f_x(x,y,z)\cdot(x^2-y^2) - \\ - f_z(x,y,z)\cdot(z^2-y^2),$$

where

$$f_n(x,y,z) = \frac{\alpha_n}{[p_n^{a_n} + \delta_n^{a_n}]^{\frac{ac_n}{a_n}}}, \qquad (14)$$

α_n, δ_n, a_n, ac_n are constants and p_n^2 is the square of the softened radius given by $p_n^2 = x^2 + y^2 + z^2 + \epsilon^2$ when $n = 0$, or $p_n^2 = x^2 + y^2 + z^2 + 2\cdot\epsilon^2$ for $n = x, z$. The adopted value for the softening parameter is $\epsilon \simeq 0.01$ for any n. The functions $f_n(x,y,z)$ were computed through a quadrupolar N–body code for 10^5 particles, which allowed the authors to write them in a general fashion given by Eq. (14). The adopted values for the constants α_n, δ_n, a_n and ac_n are given in Table 1. For further references, see [Muzzio, Carpintero and Wachlin, 2005] and [Cincotta, Giordano and Muzzio, 2008].

The stationary character of the parameters given in Table 1 were tested by performing several fits at different times after virialization, resulting in a precision of 0.1%.

After the system had relaxed, there remained 86818 particles resembling an elliptical galaxy (the system obeying a de Vaucouleurs' law, as shown in Fig. 2 in [Muzzio, Carpintero and Wachlin, 2005]) with a strong triaxiality and a flattening that increases from the border of the system to its center (see Table I in the same paper).

Table 1. Adopted values for the coefficients of the functions f_n given by Eq. (14).

	α	a	δ	ac
$n = 0$	0.92012657	1.15	0.1340	1.03766579
$n = x$	0.08526504	0.97	0.1283	4.61571581
$n = z$	−0.05871011	1.05	0.1239	4.42030943

The obtained triaxial potential has semi–axes X, Y, Z satisfying the condition $X > Y > Z$, and its minimum, which is close to -7, matches the origin. As expected, the potential is less flattened than the mass distribution (see Table I in [Muzzio, Carpintero and Wachlin, 2005]).

As we mentioned at the beginning of this section, the potential seems to provide a useful realistic scenario to test the `LP-VIcode` and the FMFT. Thus, in the next subsection, we describe how we proceed (in order) to compare both techniques as chaos detection tools.

3.2 Comparative evaluation of the FMFT and the SEILCE as global chaos detection techniques

3.2.1 Preliminaries. Herein we apply a spectral analysis method, the FMFT, and a CI, the SEILCE (one of the indicators in the library of the `LP-VIcode`) to two regions on the energy surface -0.7 of the potential described in Section 3.1. In order to compare both techniques as chaos detection tools we apply the FMFT and the SEILCE to a few samples of initial conditions in the stationary space and in the $x_0 - z_0$ start space of the self-consistent triaxial stellar model.

There are several ways to compare chaos detection tools. Our choice is to determine which technique offers the most detailed phase space portrait using the same integration time. Therefore, we must first determine an integration time by which the techniques (at least for most of the initial conditions of the samples) are out of a transient regime; otherwise, we will obtain unreliable phase space portraits.

We will consider a time of 10^3 characteristic times[3] to keep the LI out of the transient interval, as the authors did in [Maffione, Giordano and Cincotta, 2011a]. That is, a convergent LI is the criterion used (in order) to yield reliable values of the CIs, in particular of the MEGNO/SEILCE indicators. From [Maffione, Giordano and Cincotta, 2011a] we know that for the energy surface -0.7, the characteristic time is ~ 7 u.t. So, (in order) to obtain reliable values for the CIs previously mentioned, the integration time must be 7×10^3 u.t.

The FMFT indicates regular motion when the fre-

[3] We approximate this time-scale as the period of the axial orbit on the semi-major axis X of the model.

quencies do not change in time, i.e. the orbit is confined within a torus, which is well defined by a set of N frequencies (where N is the number of the d.o.f. of the system). However, if the orbit is chaotic, there is a variation in the frequencies. This lack of constancy in time means that the orbit is not confined within a torus[4]. The precision on the computation of the frequencies is a key parameter, because the FMFT might not show a variation of the frequencies in time and thus, it might not be able to distinguish chaotic from regular orbits. Then, to determine such a precision and the efficiency in describing the phase space portraits of the triaxial model for the FMFT, we use the same final integration time used with the SEILCE, i.e. 10^3 periods, which is enough to stabilize the LI for most of the initial conditions of the samples.

Finally, the equations of motion and their first variationals are integrated for a final integration time of 7×10^3 u.t. in the case of the SEILCE. For the FMFT, we compare the computation of the fundamental frequencies in two 50% ([Wachlin, Ferraz-Mello, 1998] overlapping time intervals, (in order) to estimate possible variations in the frequencies. The first interval goes from 0 u.t. to 7×10^3 u.t., and the second one, from 3.5×10^3 u.t. to 1.05×10^4 u.t.

We apply the SEILCE and the FMFT to 624100 orbits in the region of the stationary space and to 596258 orbits in the region of the $x_0 - z_0$ start space.

The integration of the equations of motion, which are necessary to compute the frequencies with the FMFT, was carried out with the `taylor` package ([Jorba and Zou, 2005]), which proved to be a very convenient tool for the model under analysis (see D12). The precision required for the phase space coordinates was of 10^{-15}.

On the other hand, the integrations for the LI and the MEGNO/SEILCE were carried out with the DOPRI8 routine (see Section 2.4), which it is more efficient than `taylor` in the case of the simultaneous integration of both the equations of motion and their variational equations for the self-consistent triaxial stellar model (we refer to D12 for further details). The energy preservation with DOPRI8 was of the order of $\sim 10^{-13}$, 10^{-14}.

The following configuration was used for all the computations included in this paper: *a)* Hardware: CPU, 2 x Dual XEON 5450, Dual Core 3.00GHz; M.B., Intel S5000VSA; RAM, 4GB(4x1GB), Kingston DDR–2, 667MHz, Dual Channel. *b)* Software: gfortran 4.2.3.

3.2.2 The experiment. In order to use the FMFT as a chaos detection tool, we compute the quantity $\log(\Delta F)$ ([Wachlin, Ferraz-Mello, 1998]). The $\log(\Delta F)$ is defined as $\Delta F \equiv |\nu_x^{(1)} - \nu_x^{(2)}| + |\nu_y^{(1)} - \nu_y^{(2)}| + |\nu_z^{(1)} - \nu_z^{(2)}|$, where $\nu_j^{(i)}$ is the fundamental frequency computed with the FMFT and associated with the degree of freedom j ($j = x, y, z$) for the interval (i), with $i = 1, 2$ (the two overlapping time intervals). Besides, we must have all the fundamental frequencies computed for every orbit on both intervals and this is not the general case for every orbit. Thus, the phase space portraits of the $\log(\Delta F)$ finally consist of 622521 orbits on the stationary space and 594690 orbits on the $x_0 - z_0$ start space.

In Fig. 1 we present the SEILCE (left panels) and the $\log(\Delta F)$ (right panels) values for the region on the stationary space (top panels) and for the region on the $x_0 - z_0$ start space (bottom panels) of the triaxial model under analysis.

Although the SEILCE and the FMFT show similar results on the stationary space (top panels of Fig. 1), the latter includes a high amount of spurious structures[5] on the $x_0 - z_0$ start space (bottom right panel of Fig. 1). This spurious structures jeopardize the choice of a threshold value in order to identify regular and chaotic orbits due to an unclear separation of the different kind of motions. On the contrary, with a variational indicator as the SEILCE (bottom left panel of Fig. 1), this classification into regular and chaotic motion seems to be more natural and thus, more efficient. Nevertheless, if in the $x_0 - z_0$ start space we take as chaotic orbits those which preserve 4 decimal digits or fewer in their computed fundamental frequencies with the FMFT, we recover the phase space portrait obtained by the SEILCE.

This kind of results, where the distinction between chaotic and regular motion is not as clear as the one given by variational indicators like the SEILCE, makes the FMFT a less reliable indicator when we study the global dynamics of a divided phase space.

The process used to determine the chaoticity or regularity of the orbits by means of the FMFT is standard. Then, the somehow inaccurate descriptions of the portraits of divided phase spaces might be basically due to a high sensitivity of the method with its parameters.

As regards the computing times, the SEILCE (one of the fastest CIs, together with the FLI and the MEGNO), took ~ 670 hs for an integration time of 7×10^3 u.t. and for 624100 orbits on the stationary space. For the 594690 orbits on the $x_0 - z_0$ start space, the CI took ~ 330 hs.

Although the computing of the fundamental frequencies with the FMFT is quite fast, the determination of the $\log(\Delta F)$ is time consuming. For instance, for the generation of the right panels of Fig. 1, two 50% overlapping time intervals of 7×10^3 u.t. each were necessary. In other words, the integration of the equations of motion was performed for a total time interval of 1.05×10^4 u.t. in order to have the frequencies computed after 10^3 periods in both intervals, the same amount of periods used with the SEILCE. Finally, the

[4] For further details on the FMFT, refer to [Sidlichovský and Nesvorný, 1996]. Herein, we simply describe how the indicator distinguishes between chaotic and regular motion, because it is needed (in order) to compare its performance with the variational tool, the SEILCE.

[5] Some of them due to the Moiré phenomenon, which is common with methods using the discrete Fourier transform ([Barrio, Blesa and Serrano, 2009]).

time taken by the $\log(\Delta F)$ was ~ 885 hs. for the stationary space and ~ 450 hs. for the $x_0 - z_0$ start space. Therefore, the computing speed of the fundamental frequencies by the FMFT is lost against the whole process involved in the determination of the variation of the frequencies with the $\log(\Delta F)$. In fact, the computing of the $\log(\Delta F)$ is necessary to distinguish between regular and chaotic orbits with the FMFT and thus, the FMFT as a global chaos indicator turns out to be slower than the SEILCE (and other similar fast CIs).

In the next section we consider the FMFT as an appropriate method for the determination of the fundamental frequencies only of the regular orbits as well as an efficient tool to determine the resonant map of the system. Furthermore, we use the FMFT as an complement to the `LP-VIcode` in order to depict the global picture of the stationary phase space.

4 Complementary use of the `LP-VIcode` and the FMFT

The analysis by means of the LI, the MEGNO/SEILCE and the FMFT of the stationary space of the triaxial potential of [Muzzio, Carpintero and Wachlin, 2005] for different energy surfaces gives us enough information to shortly discuss the advantages of using both types of techniques together, i.e. CIs (within the `LP-VIcode`) and spectral analysis methods (with the FMFT).

4.1 The contribution of the `LP-VIcode`

We consider samples of 1000444 initial conditions for the energy surfaces defined by the constant values -0.1 and -0.7; the integration times are of 1.17×10^5 u.t. (for the energy surface -0.1 the period of the semi-major axis orbit is ~ 117 u.t.) and 7×10^3 (see Section 3.2), respectively . As the computing times become critical in the experiment, we select, from the `LP-VIcode`, CIs of low computational cost: the LI and the MEGNO/SEILCE (the FLI/OFLI could be an equal efficient alternative).

The corresponding phase space portraits are presented in Fig. 2, left panel for the energy surface -0.1 and right panel for the energy surface -0.7.

The SEILCE shows a very good performance in describing the phase space portraits corresponding to a strongly divided phase space like the present one. Nevertheless, as it has not a natural way to determine a threshold value to distinguish chaotic from regular orbits, we have to estimate it (in order) to study the phase space portraits presented by the SEILCE in Fig. 2.

To determine such threshold for the SEILCE, we can calibrate the CI in order to obtain similar percentages of chaotic and regular orbits than those obtained with other confident CI with a defined threshold. The MEGNO is the first alternative due to the fact that the SEILCE needs its computation. However, as the MEGNO shows a high sensitivity with its asymptotically theoretical threshold (see e.g. M11; D12), it is not reliable to be used to calibrate other indicators. Therefore, we use other indicator already implemented in the `LP-VIcode`.

As aforementioned, the computing time is a key variable in the experiment, and thus, the LI is the CI of least computational cost given a fixed total integration time. Moreover, the indicator has a theoretical threshold value to start with: $\ln(T)/T$, with T being the total integration time. Starting with the theoretical approximation of the threshold, we calibrate it by inspection and find appropriate threshold values for the LI for both energy surfaces. Finally, the threshold of the SEILCE is estimated by an iterative process, which is stopped when the percentage of chaotic orbits best approximates the percentage of the chaotic component yielded by the LI.

In Table 2 we present, from left to right, the energy surface, the threshold value (V_c) estimated for the LI, the corresponding percentage of chaotic orbits, the estimated threshold value for the SEILCE and the corresponding percentage of chaotic orbits.

Table 2. For both energy surfaces considered on the stationary phase space (i.e. -0.1 and -0.7): the threshold value used for the LI, the percentage of the chaotic component given by the LI, the estimated threshold value for the SEILCE and the corresponding percentage of the chaotic component are detailed.

Energy	V_c (LI)	Chaos (%) -LI	V_c (SEILCE)	Chaos (%) -SE
-0.1	1.2×10^{-4}	$\sim 71.46\%$	1.4×10^{-5}	$\sim 66.83\%$
-0.7	1.7×10^{-3}	$\sim 65.09\%$	2.7×10^{-4}	$\sim 62.87\%$

Independently of the energy surface considered, the chaotic component dominates the phase space portraits (columns 3 and 5 of Table 2). However, as we move to more negative energy surfaces (-0.7), the regular component increases. The variation is not important along the energies considered, though.

On the left panel of Fig. 2, we observe that the chaotic and regular components are almost separated. On the one hand, we have the chaotic component fully connected for values of $p_{x_0} \lesssim 1.7$, and the region of regular orbits for values of $p_{x_0} \gtrsim 1.7$, except for some structures which arise from the border of the energy surface and enter the regular component. Furthermore, these structures multiply themselves as we go to more negative energies (more bonded regions of the potential). These structures are resonances that overlap with each other, and start to populate the regular component. We can also observe a division inside the chaotic component, where the connected chaotic domain move back to lower values of p_{x_0}, giving place to another chaotic domain characterized by a regime of resonance overlap and by a lower Lyapunov exponent (notice the

different colours). On the right panel of Fig 2, for an energy surface of -0.7, the resonances fill the regular component; strong resonances in the chaotic domains are also observed. The most remarkable is the one which lies around $p_{x_0} \sim 0.5$.

Given a global portrait as the one shown by means of the SEILCE, with a variational indicator we can visualize many phenomena such as how the chaotic and regular components interact, where the resonances appear and how they overlap to generate chaotic regions. However, we should make a great effort with the CIs if we need more detailed information because we need the resonant map to understand many of the causes of such phenomena.

In order to obtain the resonant map, the time evolution of the CIs which can provide information about the dimensionality of the torus on which the regular orbits lie (like the GALIs) can be analyzed, and thus, infer the resonances to which they belong. There is another way to identify the periodic orbits (e.g. using the OFLI) and analyze their stability (as done in [Cincotta, Giordano and Muzzio, 2008] with the MEGNO) in order to search for orbital families generated by perturbations to such parent periodic orbits in nearby regions. However, this process could be very slow because the CIs are not the best suited for the task.

It remains to apply the method of spectral analysis, i.e. the FMFT, to improve the study of the regular component with the associated resonant map, and thus, complement the information given by the SEILCE (also assisted by the LI).

4.2 The contribution of the FMFT

We use the FMFT to compute the frequencies of a representative sample of regular orbits and determine the resonant map of the stationary space studied in Section 4.1 by means of the SEILCE.

We first need to identify the sample of regular orbits to apply the FMFT. Such a sample consists of orbits that are simultaneously classified as regular orbits by the MEGNO and the LI. We call this sample "A".

Having the representative sample "A" of regular orbits, we integrate the equations of motion for 3×10^2 characteristic times (which gives us enough precision) in order to compute the frequencies with the FMFT. We are not able to compute the three fundamental frequencies for all the orbits of sample "A" but for most of them. We call this reduced sample of regular orbits with the three fundamental frequencies computed sample "B". Finally, we use sample "B" to compute the commensurabilities and identify the resonance web.

We consider as resonant orbits those whose resonant vector $\vec{m} \in \mathbb{Z} - \{\vec{0}\}$ satisfies the relation: $\vec{m} \cdot \vec{\nu} < 10^{-6}$ with $\vec{\nu}$ being the frequency vector. The value 10^{-6} is an estimated value according to the best fit between the resonance web and the description of the phase space previously given by the CIs (Section 4.1). We separate the resonances according to the d.o.f. involved, i.e. into resonances between 2 and 3 d.o.f. In the case of the resonances between 2 d.o.f., we only searched for those of highest order, i.e. iterating until 2×10^2 on each d.o.f. Lastly, we sorted them by their resonant vector's absolute value which yields information about the width and importance of the resonance ([Reichl, 2004]).

In Table 3 we show, for each energy surface and a total of 1000444 initial conditions, the number of orbits in the representative sample "A", the total time used with the FMFT to compute the fundamental frequencies, the number of orbits in the reduced sample "B" and the number of orbits in resonance (with 2 or 3 d.o.f. involved).

Table 3. For each energy surface (i.e. -0.1 and -0.7) on the stationary space, the following information is provided: the number of orbits in the representative sample "A", the integration time used by the FMFT to determine the fundamental frequencies, the number of orbits in the reduced sample "B" and lastly, the number of orbits in resonance between 2 or 3 d.o.f.

Energy	Sample "A"	Time interval	Sample "B"	In resonance
-0.1	7.2426×10^4	3.51×10^4	7.2295×10^4	1.315×10^3
-0.7	7.2948×10^4	2.1×10^3	7.2781×10^4	1.773×10^3

Notice in Table 3 that the percentage of orbits in resonances is not high and is similar for both surfaces: $\sim 1.82\%$ for -0.1 and $\sim 2.43\%$ for -0.7 in the stationary space.

In Figure 3 we show the resonant maps corresponding to the energy surfaces -0.1 (left panel) and -0.7 (right panel) of the stationary space of the self-consistent triaxial stellar model of elliptical galaxy under study. The resonant map corresponding to the energy surface -0.1 shows populated regions of resonant orbits near the chaotic component and close to the border of the corresponding energy surface. However, the resonant orbits are of very low order (i.e. $|\vec{m}|^2 \gtrsim 10^3$). On the other hand, on the right panel of Figure 3, we show the results for the energy surface -0.7 and we observe a highly compact resonance of high order in the chaotic domain. In order to identify such a resonace we compute the rotational numbers with the fundamental frequencies given by the FMFT and find that the resonance is between 2 d.o.f., the $4:3$ (x:y) resonance.

As we can see from the experiment, the variational indicators such as the LI and the couple MEGNO/SEILCE (computed with the `LP-VIcode`) and the spectral analysis methods such as the FMFT work remarkably well as complementary methods.

5 Discussion

From all the studies carried on in this paper, we might conclude that having a large indicators diversity is es-

sential to have a precise description of a dynamical system. Thus, in the first part of this work we presented the alpha version of the LP−VIcode. A code that is on a developing stage but which has already proved its value. The purpose of the LP−VIcode is to efficiently arrange together a great variety of CIs in order to have at hand several dynamical tools to study a given dynamical system. The arrangement has not considered spectral analysis methods yet, since the original idea was to reduce the CPU time when computing several variational indicators. Nevertheless, this is not discarded for future implementations.

The CIs included and full functioning in this alpha version of the LP−VIcode are the following: the LI, the RLI, the SALI, the GALI$_k$, the MEGNO, the SEILCE, the FLI, the OFLI, the OFLI$_2^{TT}$, the D, the SSNs and the APLE (Section 2.1). They can be computed separately or within units, i.e., in order to reduce the CPU time economizing similar processes they have in their computing routines (Section 2.2).

In the second part of this work, we use the availability of the CIs given by the LP−VIcode to compare different sort of tools for dynamical analysis. On the one hand, we have the CIs which are based on the concept of local exponential divergence and follow the evolution of the deviation vectors. On the other hand, we have the spectral analysis methods, which require the integration of the equations of motion to compute, e.g., the frequencies of regular orbits.

According to previous papers such as [Barrio, Blesa and Serrano, 2009], we find that the complementary use of such techniques, the CIs and the spectral analysis methods, is a very efficient way to gather dynamical information (Section 4).

Here, we show that the SEILCE (a CI) works better than the FMFT (a spectral analysis method) as a global chaos detection tool (Section 3.2) to describe the divided phase space of the self-consistent triaxial stellar dynamical model resembling and elliptical galaxy (Section 4.1). The fundamental frequencies of the regular orbits easily provided by the FMFT allow a fast building of the resonance web and thus, a quick understanding of many phenomena described in the phase space portraits given by the CI (Section 4.2).

Finally, in view of the present succesful applications of the LP−VIcode, there are still many improvements to be made to the code. Among the main goals, we can mention the following:

To continue increasing the record of CIs in the library of the code.
To incorporate routines to compute diffusion rates, in order to take advantage of the many computations done by the code.
To recode it in FORTRAN 90.
To make the code independent of the integrator routine.
To make the code independent of the model, using symbolic manipulation programs to decode the differential equations and implement them automatically.

Our aim is to release a stable version of the LP−VIcode with all those goals implemented and offer the code to public domain, so that the interested community may collaborate including their own chaos detection tools and/or improve the ones already implemented.

References

Antonopoulos, Ch., Vasileios, B. & Bountis, T. 2010, Phys. Rev. E., 81, 016211.

Barrio, R. 2005, Chaos, Solitons and Fractals, 25, 711-726.

Barrio, R., Blesa, F. & Serrano, S. 2009, Physica D, 238, 1087-1100.

Barrio, R., Blesa, F. & Serrano, S. 2010, Int. J. Bifurcations and Chaos, 20, 1293-1319.

Benettin, G., Galgani, L. & Strelcyn, J. 1976, Phys. Rev. A, 14(6), 2338-2345.

Benettin, G., Galgani, L., Giorgilli, A. & Strelcyn, J. 1980, Meccanica 15 Part I, 9-20; Part II, 21-30.

Binney, J. & Spergel, D. 1982, Ap. J., 252, 308-321.

Bountis, T.C. & Skokos, Ch. 2006, 561, 173-179.

Carpintero, D. 2008, MNRAS, 388, 1293-1304.

Cincotta, P. & Simó, C. 2000, Astron. Astrophys, 147, 205-228.

Cincotta, P., Giordano, C. & Sim, C. 2003, Physica D., 182, 151-178.

Cincotta, P., Giordano, C. & Muzzio, J.C. 2008, Discrete and Continuous Dynamical Systems B., 10, 439-454.

Compère, A., Lematre, A. & Delsate, N. 2011, CeMDA, 112, 75-98.

Contopoulos, G. & Voglis, N. 1996, CeMDA, 64, 1-20.

Contopoulos, G. & Voglis, N. 1996, Astron. & Astrophys, 317, 73-81.

Contopoulos, G., Voglis, N., Efthymiopoulos, Ch., Froeschlé, Cl., Gonczi, R., Lega, E., Dvorak, R. & Lohinger, E. 1997, CeMDA, 67, 293-317.

Darriba, L., Maffione, N., Cincotta, P. & Giordano, C. (Accepted), IJBC (D12)

Fouchard, M., Lega, E., Froeschlé, Ch. & Froeschlé, Cl 2002, 83, 205-222.

Froeschlé, Cl. 1984, CeMDA, 34, 65-115.

Froeschlé, Cl., Gonczi, R. & , Lega, E. 1997a, Planet. Space Sci., 45, 881-886.

Froeschlé, Cl., Lega, E. & Gonczi, R. 1997b, CeMDA, 67, 41-62.

Froeschlé, Cl. & , Lega, E. 1998, Astron. Astrophys., 334, 355-362.

Froeschlé, Cl. & , Lega, E. 2000, CeMDA, 78, 167-195.

Froeschlé, Cl. & Lega, E. 2006, B.A. Steves et al (eds) Chaotic Worlds: from Order to Disorder in Gravitational N-Body Dynamical Systems, 131-165.

Gayon, J. & Bois, E. 2008, Astron. & Astrophys., 423, 745-753.
Hinse, T., Christou, A., Alvarellosn, J. & Gózdziewski, K. 2010, MNRAS, 404, 837-857.
Goździewski, K., Konacki, M. & Maciejewski, A. 2005, Ap. J., 619, 1084-1097.
Guzzo, M., Lega, E. & Froeschlé, Cl. 2002, Physica D., 163, 1-25.
Hénon, M. & Heiles, C. 1964, Astronom. J., 1, 73-79.
Hinse, T., Christou, A., Alvarellosn, J. & Gózdziewski, K. 2010, MNRAS, 404, 837-857.
Jorba, À. & Zou, M. 2005, Experimental Mathematics, 14, 99-117.
Laskar, J. 1990, Icarus, 88, 266-291.
Laskar, J., Froeschlé, Cl. & Celetti, A. 1992, Physica D, 56, 253-269.
Lega, E. & Froeschlé 2001, CeMDA, 81, 129-147.
Lega, E., Guzzo, M. & Froeschlé, Cl. 2010, CeMDA, 107, 115-127.
Lemaître, A., Delsate, N. & Valk, S. 2009, CeMDA, 104, 383-402.
Lukes-Gerakopoulos, G., Voglis, N. & Efthymiopoulos, Ch. 2008, Physica A, 387, 1907-1925.
Maffione, N., Giordano, C. & Cincotta, P. 2011a, Int. J. of Nonlinear Mech., 46, 23-34.
Maffione, N., Darriba, L., Cincotta, P. & Giordano, C. 2011b, CeMDA, 111, 285-307. (M11)
Manos, T. & Athanassoula, E. 2011, MNRAS, 415, 629-642.
Muzzio, J. 2006, CeMDA, 96, 85-97.
Muzzio, J., Carpintero, D. & Wachlin, F. 2005, CeMDA, 1, 173–190.
Paleari, S., Froeschlé, Cl. & Lega, E. 2008, CeMDA, 102, 241-254.
Papaphilippou, Y. & Laskar, J. 1996, Astron. & Astrophys., 307, 427-449.
Prince, P. & Dormand, J. 1981, J. Comput. Appl. Math., 35, 67-75.
Reichl, L. 2004, The transition to Chaos. Conservative classical systems and quantum manifestations. Second Edition. Springer-Verlag.
Sándor, Z., Érdi, B. & Efthyimiopoulos, C. 2000, CeMDA, 78, 113-123.
Sándor, Z., Érdi, B., Széll, A. & Funk, B. 2004, CeMDA, 90, 127-138.
Sándor, Z., Süli, Á., Érdi, B., Pilat-Lohinger, E. & Dvorak, R. 2007, MNRAS, 375, 1495-1502
Schwarzschild, M. 1993, Ap. J., 409, 563-577.
Sidlichovský, M. & Nesvorný, D. 1996, CeMDA, 65, 137-148.
Skokos, Ch. 2001, J Phys A-Math Gen., 34, 10029-10043.
Skokos, Ch. 2010, Lect. Notes Phys., 790, 63-135
Skokos, Ch., Bountis, T. & Antonopoulos, Ch. 2007, Physica D., 231, 30-54.
Skokos, Ch., Bountis, T. & Antonopoulos, Ch. 2008, The European Physical J. Special Topics, 165, 5-14.
Széll, Érdi, B., Sándor, Z. & Steves, B. 2004, MNRAS, 347, 380-388.
Tancredi, G., Sánchez, A. & Roig, F. 2001, Astronom. J., 121, 1171-1179.
Todorović, N., Lega, E. & Froeschlé, Cl. 2008, CeMDA, 102, 13-27.
Voglis, N. & Contopoulos, G. 1994, J. Phys. A: Math. Gen., 27, 4899-4909.
Voglis, N., Contopoulos, G. & Efthymiopoulos, Ch. 1998, Phys. Rev. E., 57, 372-377.
Voglis, N., Contopoulos, G. & Efthymiopoulos, C. 1999, CeMDA, 73, 211, 220.
Wachlin, F. & Ferraz-Mello, S. 1998, MNRAS, 298, 22

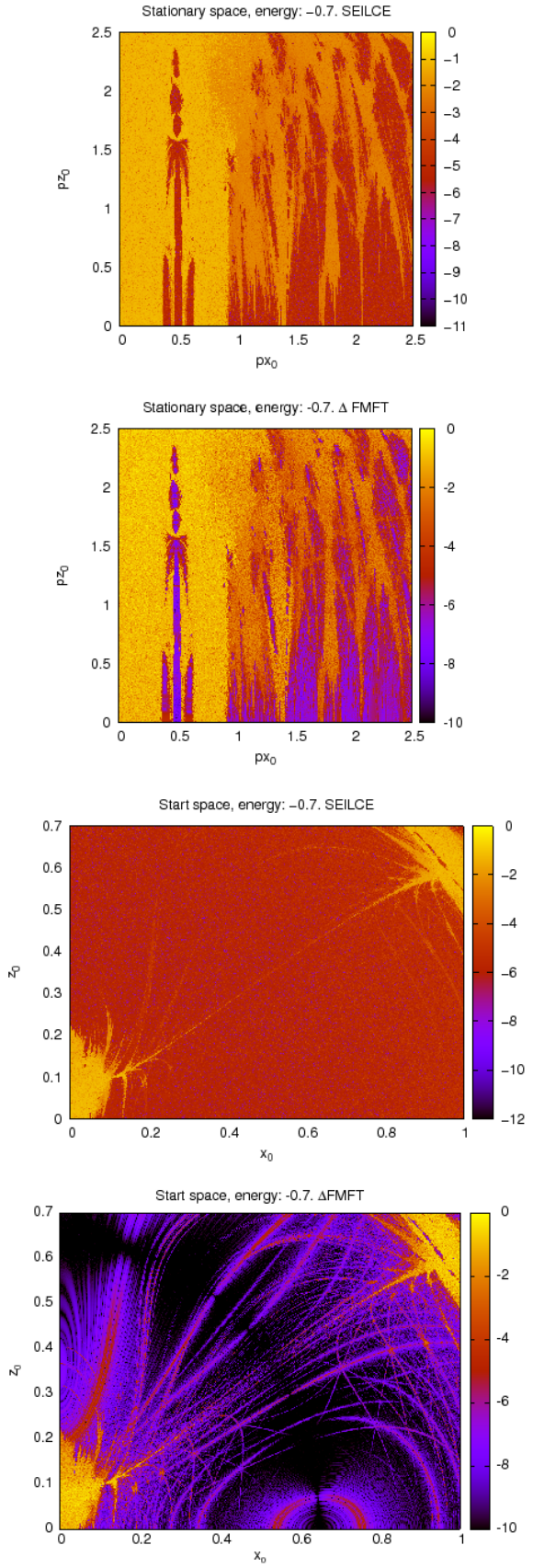

Figure 1. Phase space portraits of the stationary space with 624100 initial conditions (top left panel) and of the $x_0 - z_0$ start space with 596258 initial conditions (bottom left panel), using the values of the SEILCE integrated for 7×10^3 u.t. Right panels, idem but with 622521 and 594690 initial conditions (top and bottom right panels, respectively), using the $\log(\Delta F)$ integrated on two overlapping time intervals of 7×10^3 u.t. each. The values of the SEILCE and the $\log(\Delta F)$ are in logarithmic scale.

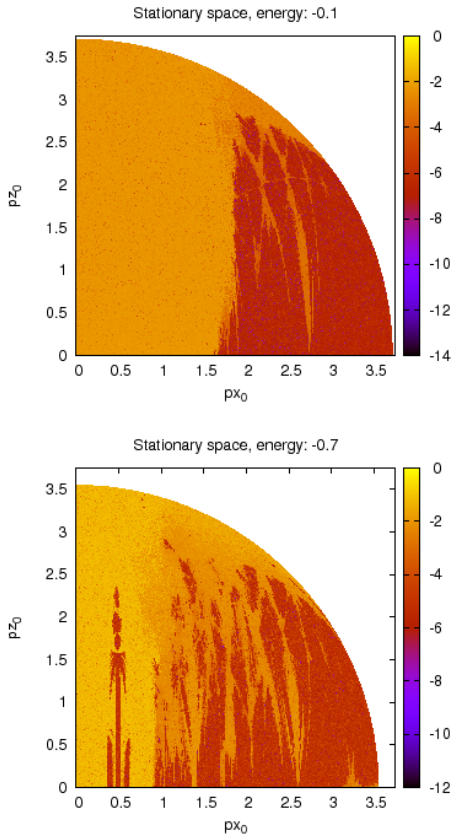

Figure 2. Phase space portraits by means of the SEILCE for the stationary space of the triaxial model, integrating 1000444 orbits for 10^3 periods on two energy surfaces. On the left panel, for the energy surface -0.1 within a time interval of 1.17×10^5 u.t and on the right panel, for the energy surface -0.7 within a time interval of 7×10^3 u.t. The values of the SEILCE are in logarithmic scale.

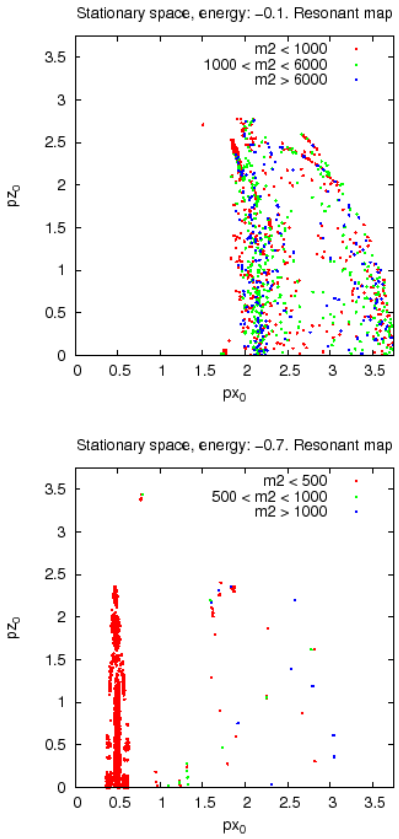

Figure 3. Resonant maps for both energy surfaces on the stationary space. We sort the resonances by the value $m2 = |\vec{m}|^2$. Left panel for the energy surface -0.1 and right panel for the energy surface -0.7.